Crack shapes and crack driving force distributions for naturally growing fatigue cracks

Mikel Escalero[a,*], Miguel Muniz-Calvente[b], Haritz Zabala[a], Iker Urresti[a]

[a] *Ikerlan Technology Research Center, Basque Research and Technology Alliance (BRTA). Pº J.M. Arizmendiarreta, 2, 20500 Arrasate-Mondragón, Spain.*
[b] *Department of Construction and Manufacturing Engineering, University of Oviedo. C\Pedro Puig Adam, s/n, 33204 Gijón, Spain.*

Abstract

Extensive literature supports that fatigue cracks tend to a stable stage driven by an iso crack driving force (CDF) distribution that produces a quasi-constant crack shape. Here fatigue crack growth is studied by two means: 1) a finite element simulation based on crack-tip opening displacements and remeshing and mapping strategies and 2) a theoretical analysis based on the multiple-degree-of-freedom scheme and power-law crack growth relationships. Contrary to the literature, naturally growing fatigue cracks are found to converge towards a quasi-constant crack-shape regime promoted by a non-iso CDF distribution that depends on material properties and the stable crack shape.

Keywords: Crack shape, crack driving force, fatigue crack growth, predictions

*Corresponding author
Email address: mescalero@ikerlan.es (Mikel Escalero)

Nomenclature

Latin characters

a	Crack length (mm)
$\mathrm{d}a/\mathrm{d}N$	Crack growth rate (mm/cycle)
K	Stress intensity factor ($\mathrm{MPa\,mm^{1/2}}$)
P	Load (N)
s	Slope of the crack front (-)
U	Ratio between effective and total stress intensity factor ranges (-)
W	Width (mm)
z	Location in thickness (mm)

Greek characters

β	Proportionality constant between $\Delta\mathrm{CTOD_p}$ and $\mathrm{d}a/\mathrm{d}N$ (-)
σ	Stress (MPa)

Subscripts

$()_{\mathrm{eff}}$	Effective
$()_{\mathrm{end}}$	End
$()_{\mathrm{ini}}$	Initial
$()_{\mathrm{max}}$	Maximum
$()_{\mathrm{mid}}$	Midplane
$()_{\mathrm{op}}$	Opening
$()_{\mathrm{p}}$	Plastic
$()_{\mathrm{sur}}$	Surface
$()_{\mathrm{y}}$	Yield

Abbreviations

CDF	Crack Driving Force
CT	Compact Tension
CTOD	Crack Tip Opening Displacement
FCG	Fatigue Crack Growth
FE	Finite Element
PICC	Plasticity Induced Crack Closure

1. Introduction and motivation

Fatigue crack growth (FCG) in metallic components is driven by externally applied loads and the crack-tip plastic phenomena, such as plasticity-induced crack closure (PICC) [1, 2]. Both global (loading-related) and local (PICC-related) effects vary considerably along the crack front due to the significant stress-state variations through the thickness [3, 4], producing a crack shape evolution that has been confirmed empirically [5, 6]. Thus, naturally growing fatigue cracks, which are free from imposed restrictions, must be based on a point-wise calculation of the fracture parameters acting as the crack driving force (CDF) and a correct determination of crack shapes.

In the last decades, it has been challenging for researchers to determine CDF distributions and crack shapes. Commonly, they have done so through the finite element (FE) method, which provides the versatility to consider different crack configurations [7]. As a result, several FE approaches have been presented relying on different hypotheses. Some of these approaches calculate the crack shape evolution by neglecting PICC, others determine the evolution of the CDF by considering fixed crack shapes or imposed evolving crack shapes, yet others predict the evolution of crack shapes by resorting to simplified estimations of PICC. Finally, some explicitly calculate the CDFs accounting for PICC and determine the resulting crack shapes. These approaches and the most remarkable discoveries are reviewed below.

One of the pioneering approaches is the remeshing proposed by Lin and Smith [8–10]. This approach uses a 3D linear-elastic FE model containing the crack and iteratively advances the crack front according to a multiple-degree-of-freedom ΔK-propagation scheme that neglects PICC. Based on this approach, the literature has agreed to identify two different propagation stages [11, 12]: a transitory stage characterized by significant crack-shape changes driven by the initial non-uniform K-distribution [9], and a stable stage where the crack tends towards a converged crack shape promoted by an iso-K distribution [13], following preferred crack paths that do not depend on the initial crack [14].

Another popular approach is the node release proposed by Chermahini [15]. This approach develops the plastic wake using a 3D elastic-plastic FE model and a rigid contact surface on the fracture plane to simulate PICC, under the assumption of a fixed crack shape. Following that approach, and considering straight through-cracks, it has been found that the through-the-thickness distribution of the CDF is maintained as the crack propagates, with higher values of ΔK_{eff} in the interior than in the surface region [16]. Alternatively, Gardin et al. have calculated ΔK_{eff} distributions with two parallel FE models, one linear elastic to determine $K_{\max}$ and the other elastic-plastic (with a fracture-plane rigid surface for simulating PICC) to calculate the normalized crack opening load, $P_{\text{op}}/P_{\max}$ ($K_{\text{op}}/K_{\max} = P_{\text{op}}/P_{\max}$) [17]. They use the node release technique in the elastic-plastic FE model to propagate the crack following intermediate shapes that are assumed based on the initial straight crack and the final experimentally measured curved crack. Following their approach, Gardin et al. have identified that ΔK_{eff} stabilizes along the crack front, although some fluctuations were found and attributed to the intermediate crack-shape uncertainty [17].

Other authors have calculated crack shapes and CDF distributions by explicitly considering the interaction between the crack shape and PICC, while still applying some assumptions. Branco has improved on Lin and Smith's remeshing, by considering that only a portion U of the nominal ΔK acts effectively for a few nodes close to the surface ($\Delta K_{\text{eff}} = U \cdot \Delta K$) [12, 18]. By postulating close-to-unity

values ($0.88 < U < 1$) for those superficial nodes, Branco has identified the already commented trends in crack shapes at both the transitory and stable stages, finding a more tunneled final crack shape associated with a greater PICC at the surface [18]. Similarly, Yu and Guo have employed the remeshing combined with an analytically-estimated ΔK_{eff} ($\Delta K_{\text{eff}} = K_{\max} - K_{\text{op}}$), though they resort to a closed-form expression for the point-wise (node-to-node) calculation of the opening K (K_{op}) [19, 20]. That closed-form expression is based on an equivalent thickness conception that eliminates the arbitrary assignation of U values, but exclusively considers ideal crack shapes (e.g. semi-elliptical) and material behavior (e.g. no hardening) [20]. Following their approach, Yu and Guo have also discovered that, under applied tensile loads, different initial semi-elliptical cracks tend to crack shapes with similar aspect ratios and have achieved a high correlation with experimental beachmarks [19].

In a strict sense, only a few authors have predicted FCG by calculating CDFs that consider PICC for the particular case while predicting naturally evolving crack shapes. Many of these authors have proposed approaches that simultaneously run two geometrically identical FE models to calculate the linear elastic and elastic-plastic components of ΔK_{eff}. In particular, to keep the load history information in the elastic-plastic FE model while changing the crack shape, Hou suggests the free-front technique [21], Gozin and Aghaie-Khafri propose remeshing and mapping strategies [22], and Gardin et al. employ remeshing operations for a constant-ΔK case [23]. All three aforementioned authors (Hou, Gozin and Gardin) have contrasted the predicted shapes with experimental measurements and have reported good correlations. However, only Gardin et al. have exhaustively analyzed the evolution of the CDF distributions with crack propagation, discovering an almost constant through-the-thickness distribution of ΔK_{eff} for the stable crack, with 7% and 9% fluctuations with respect to the average values for fitted parabolic and elliptic shapes, respectively [23]. In fact, they use that iso-ΔK_{eff} distribution to declare ΔK_{eff} as the governing CDF [17].

Recently, the present authors have proposed a FCG propagation approach [24] that determines the CDF values by explicitly accounting for PICC (thus avoiding assumptions or analytical approximations for $P_{\text{op}}/P_{\max}$), which naturally builds the evolving crack shape from the local crack-advances (thus avoiding postulated or mathematically-fitted shapes). The approach, which requires a single FE model of the cracked body, 1) relies on crack-tip opening displacements that intrinsically account for plasticity-induced crack closure, 2) allows crack shape evolution by remeshing of the crack front region, 3) keeps load history by mapping the finite element results and 4) simulates crack advances by node releases. The original paper proposing this approach [24] applied it to study a cracked compact tension (CT) specimen, however, due to the high computational cost, the stable crack shape had to be analytically extrapolated based on converged intermediate CDF distributions.

In summary, the literature has made significant progress in identifying the trends in crack shapes and CDF distributions, using a wide variety of FE approaches. However, most of these approaches rely on hypotheses that may have biased the results. These hypotheses are, on one side, related to crack shapes: the assumption of constant crack shapes [15, 16], the postulation of the evolving intermediate shapes [17], or the fits with mathematical functions that force ideal shapes [23]. On the other side, the hypotheses related to CDF distributions are: the use of essentially linear elastic CDFs such as ΔK or ΔK_{eff} [8, 11, 13, 18, 23], the neglection of PICC [8, 13], the assumption of the values for the crack opening loads [18], or the determination of crack opening loads with closed-form expressions developed

under restrictive material and crack configuration hypotheses [19, 20]. Furthermore, more advanced approaches are computationally expensive, so the behavior of the crack at its stable stage has only been estimated based on partial simulation results [24].

Therefore, this work still pursues to understand the evolution of naturally growing fatigue cracks, to establish the evolution of crack shapes and CDF distributions and their relationship. To do this, the work first optimizes the authors' original approach and applies it to the mentioned CT configuration. Then, it complements the results by using a theoretical analysis that addresses generic crack shapes and various fracture parameters.

2. Finite element simulation of a naturally growing crack in CT configuration

To study the evolution of crack shapes and CDFs, the representative case of a crack growing in a CT specimen was analyzed. In particular, the growth of an initially-straight 12-mm long through-crack was simulated in a standard 2.4-mm thick CT specimen made of S275 structural steel.

2.1. FCG simulation approach

2.1.1. Original approach

The main steps for simulating FCG were the following, as described in detail in the original paper [24].

In the first place:

1. Definition of elastic-plastic FE model: An FE model of the quarter CT was built in Ansys. The mesh comprised a bulk region and a fine local region made of structured linear hexahedral elements (Figure 1a), and both regions were tied together by a bonded contact. A rigid surface was placed on the fracture plane to simulate the crack-face contact with the other specimen portion (not modeled explicitly). The local mesh had 25 elements unevenly-distributed through the thickness (see illustration in Figure 1b). Close to the crack-front, the elements were 8.56 µm x 8.56 µm in plane, with dimensions between 16 µm and 105 µm in the thickness direction. The material properties of S275 were assigned to the model, including the linear elastic properties and the Chaboche hardening behavior [24].

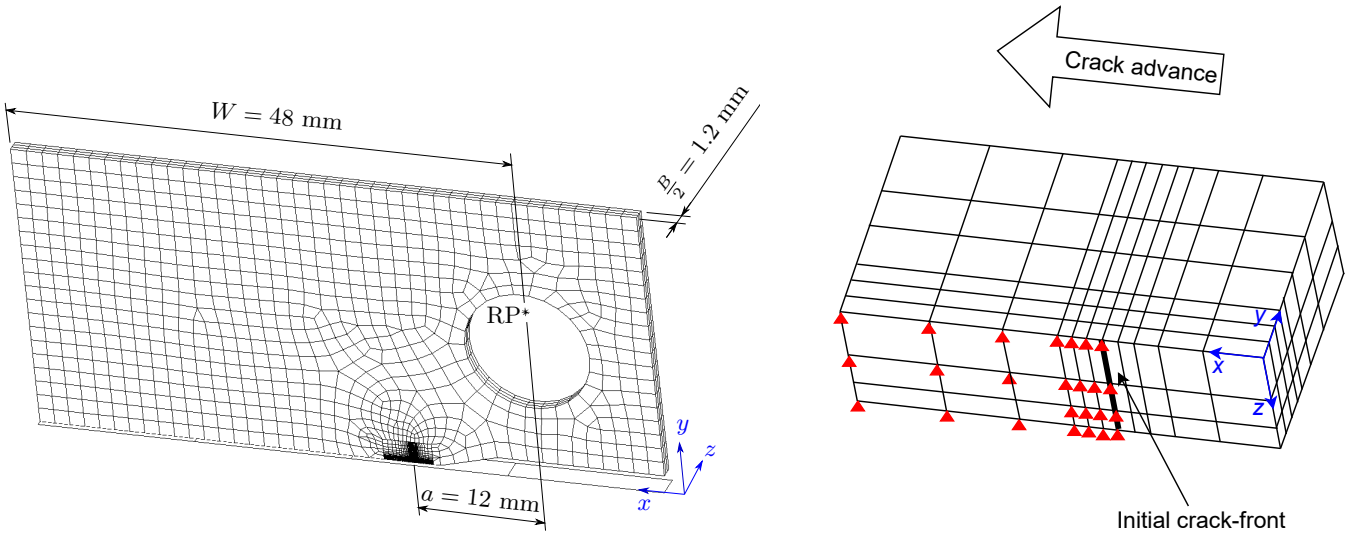

(a) Global mesh and relevant dimensions

(b) Illustration of the local mesh

Figure 1: FE model of the CT specimen.

Then, the following steps were applied repetitively for each crack advance (Figure 2), until the achievement of a quasi-constant crack shape.

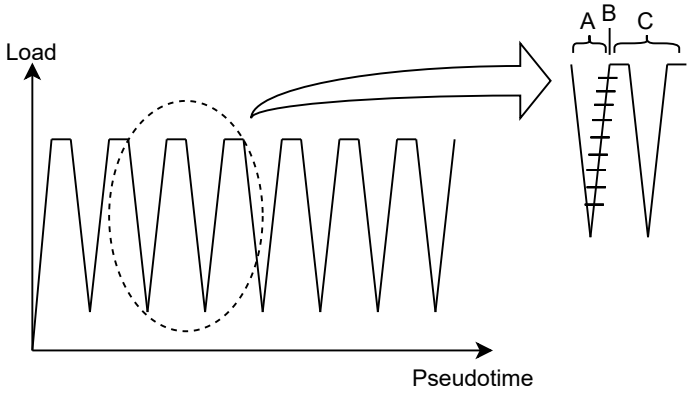

Figure 2: Cyclic load profile applied to the FE model.

2. Simulation of fatigue process (A): A complete load cycle was applied so that the material response stabilized in the crack front region. The loading step was divided into many small increments (80 in this case) to obtain smooth displacement results.
3. Calculation of crack driving force (B): CTOD-based fracture parameters were extracted using the displacements of the nodes behind the present crack front, as shown in Figure 3. In this

study, both ΔCTOD [25–28] and $\Delta\text{CTOD}_\text{p}$ [29, 30] were regarded as CDFs, motivated by their popularity in the literature.

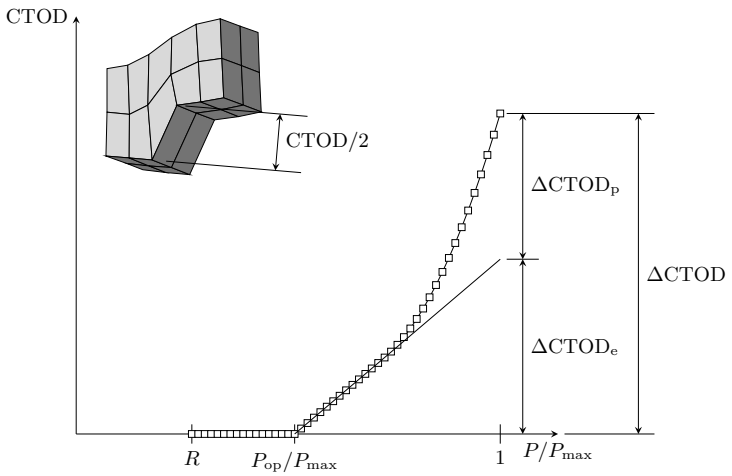

Figure 3: Determination of ΔCTOD and $\Delta\text{CTOD}_\text{p}$ from CTOD curves.

4. Determination of new crack front locations (B): The provisional location of the new crack front was obtained based on: 1) the normal directions derived from the local slopes of the present crack front and 2) the crack advances determined using the values of the CDF and the crack growth law. Initially, a surface advance of approximately 1.5 times the element size (8.56 µm) was imposed in the global propagation direction (x), to define such crack advances. As the variations from successive crack fronts decreased, that surface advance was gradually increased up to 2.5 times the element size to reduce the computational cost.
5. Local remeshing (B): The front portion of the local mesh, ahead of the present crack front, was replaced by a mesh adapted to the new crack front shape in each crack advance. That new mesh had nodes defined based on the provisional positions calculated in Step 4, and the original through-the-thickness distribution of the crack front nodes was preserved by a cubic splines interpolation. A row of nodes was placed perpendicularly behind the new crack front nodes at a distance of an element size, between the present and new crack fronts, to measure CTOD in the following crack advance.
6. Boundary conditions and results mapping (B): The boundary conditions and results were mapped from the old local mesh portion to the new one. Then, the whole FE model was solved to balance the residual forces resulting from the mismatch between the internal nodal forces calculated from the interpolated Gauss point stresses and the external nodal forces.
7. Node release (C): Finally, the nodes of the present crack front and the nodes for measuring CTOD for the new crack front were released (i.e., their normal-to-fracture-plane displacement restrictions were removed) to simulate the crack advance. A load cycle was applied between both releases (Figure 2) to avoid generating irregular crack faces.

2.1.2. Optimization of the original approach: improvements in remeshing

The FCG simulation required many crack advances to reach the stable crack-shape, so this was not fully accomplished by the present methodology following the previous remeshing strategy [24]. The problem was that the initial front portion of the local mesh had to be extremely dense, not to run out of nodes/elements ahead of the crack-front as the crack propagated. Note that crack propagation is simulated by node release, what means that every crack-advance leaves two rows of nodes/elements behind.

In this study, an improved remeshing strategy was designed to overcome the above problem. The solution was to start with a sparse front portion of the local mesh and to introduce, in each remeshing, as many additional nodes as left behind by the crack-front in each advance. This strategy still suffers from a progressive increase of the local mesh as the crack propagates, given the nodes/elements that accumulate behind the crack-front, but avoids having a heavy mesh from the beginning.

For a clearer comparison, Figure 4 shows an illustrative example of a crack propagation comprising two advances. Let us consider that 6 element rows are needed at least ahead of the crack-front for a good representation of the displacement and stress fields. Following the previous remeshing strategy, the local mesh would always have 15 rows of elements, fewer ahead and more behind each time the crack grows. In that strategy, the front portion would become less and less dense up to reaching the optimum ahead-of-crack elements (6 rows). Following the new remeshing strategy, the local mesh could start with just 6 rows of elements ahead of the crack-front. Through the propagation, more and more elements would appear behind the crack front, but ahead elements would not be consumed because each remeshing introduces new ones at each advance. Therefore, the local mesh would have 15 rows of elements only in the last step of the simulation.

Obviously, the mesh difference between strategies was much greater in the studied CT model. In fact, the computational time was reduced by a factor of 4-5, managing to complete the FCG simulation based on 75 crack advances in approximately 7 days, using a workstation with 12 cores and 128 RAM. Additionally, results were checked, finding the same tunneling evolution ($a_{\text{mid}} - a_{\text{sur}}$) with both remeshing strategies (Figure 5).

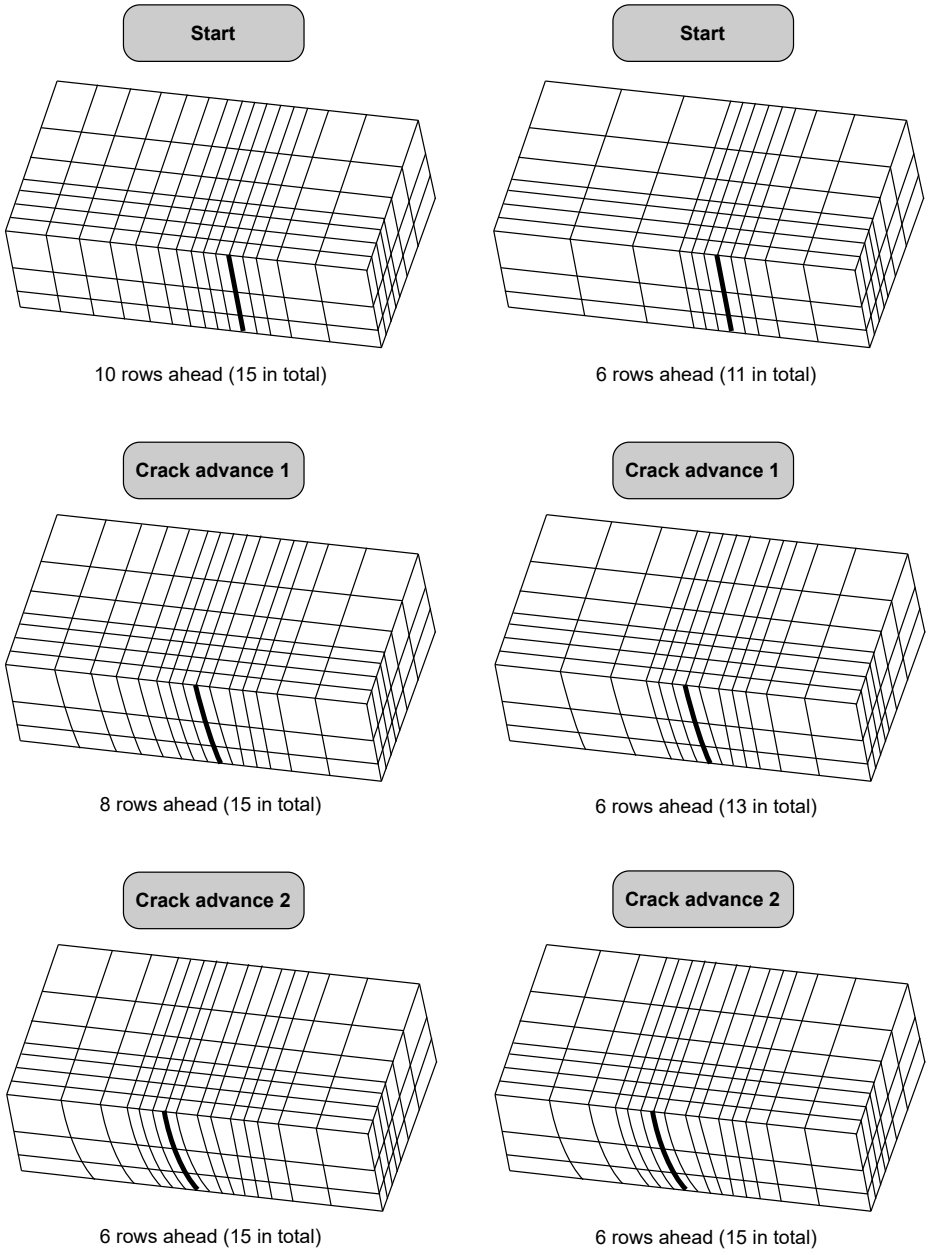

(a) Previous remeshing strategy (b) Improved remeshing strategy

Figure 4: Illustration of previous and improved remeshing strategies.

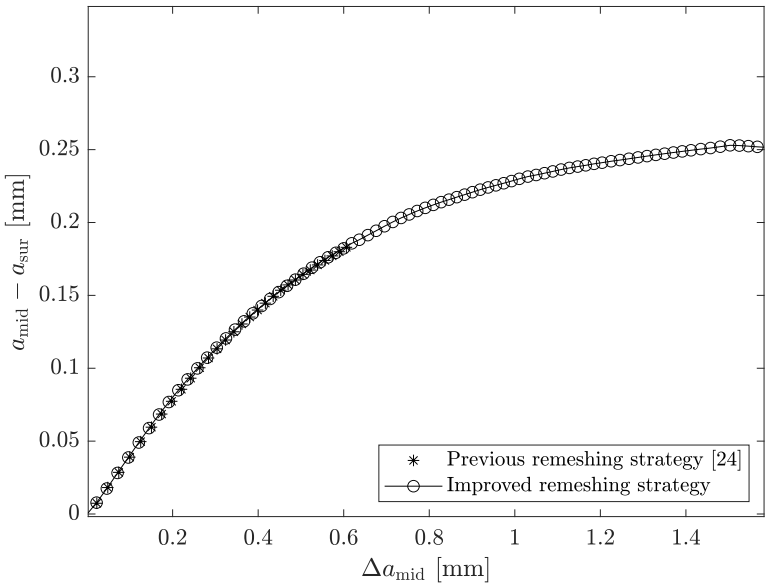

Figure 5: Evolution of the tunneling according to simulations with $\Delta\mathrm{CTOD_p}$.

2.2. Results

2.2.1. Crack shapes

Figure 6 shows the predicted beachmarks and the evolution of the crack tunneling distance ($a_{\mathrm{mid}} - a_{\mathrm{sur}}$). Under both CDFs, the initial straight crack front progressively bends, growing more at the midplane than at the surface. Branco et al. [18] have attributed this trend to a higher CDF acting at the midplane.

At the start of the propagation, the tunneling distance changes quickly, indicating significant crack shape changes. For example, by the time the crack reaches the initial plastic zone size ($r_{\mathrm{p,inimax}} =$ 190 µm) at the midplane, the tunneling distances are as high as 77 µm and 67 µm with $\Delta\mathrm{CTOD_p}$ and ΔCTOD.

As the crack propagates beyond that, the changes in tunneling distance slow down, and a practically constant tunneling distance is achieved according to both CDFs at $\Delta a_{\mathrm{mid}} \approx 1.5$ mm. Such stabilization indicates that the crack front has achieved a quasi-constant shape. The predicted values of the tunneling distance, 253 µm with $\Delta\mathrm{CTOD_p}$ and 247 µm with ΔCTOD, are close to the experimental value (264 µm) [24], presenting errors of -4.17% and -8.93%, respectively. The trends found are consistent with the literature, because studies have already numerically [17, 19] and experimentally [5, 6] demonstrated that the crack front reaches a stable shape.

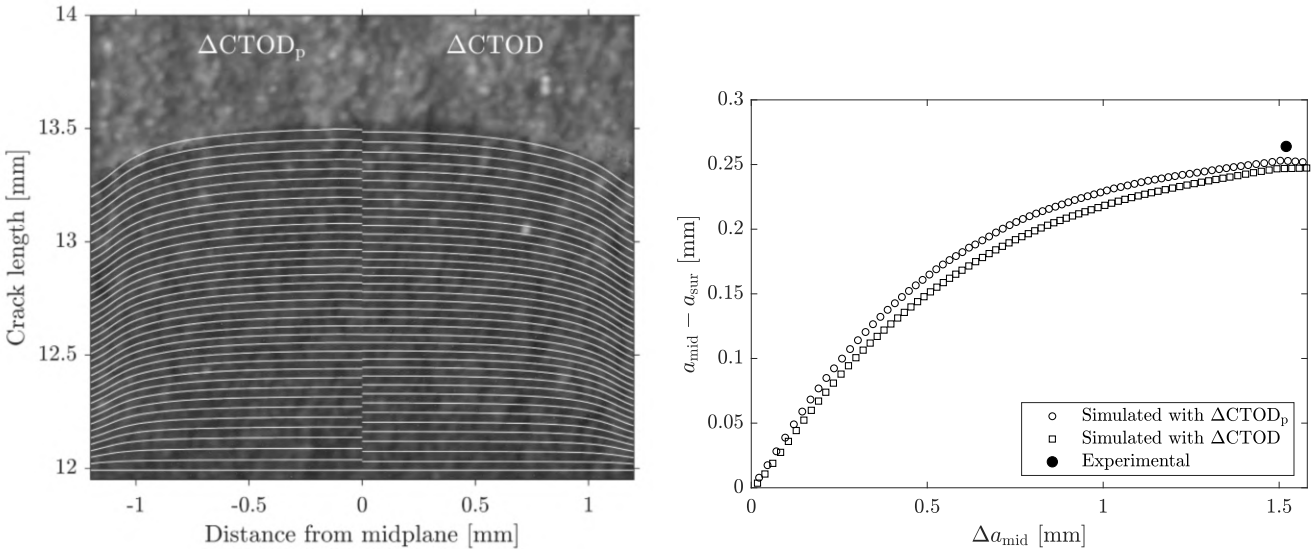

(a) Beachmarks (b) Tunneling distance

Figure 6: Predicted beachmarks and tunneling distance.

Figure 7 shows the stable crack-shapes determined at $\Delta a_{\text{mid}} \approx 1.5$ mm (the scale is distorted to highlight differences), and compares the absolute local slopes for a better discussion about shape.

The results indicate that the experimental beachmark changes more gradually through the thickness, whereas the simulated shapes are flatter in the bulk region and bend more quickly at the surface. Both CDFs yield a similar front, but in contrast with the correlation in tunneling, the result with ΔCTOD is closer to the experimental shape all along the crack-front.

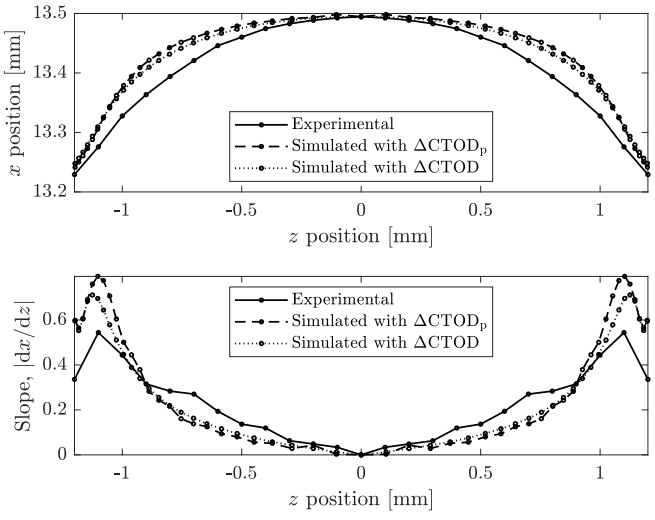

Figure 7: Numerical-experimental correlation of the experimental beachmark.

2.2.2. CDF distributions

Figure 8 shows the through-the-thickness distributions of $\Delta\text{CTOD}_\text{p}$ (left column) and ΔCTOD (right column) throughout a total crack propagation of approximately 1.5 mm ($7.89r_{\text{p,inimax}}$) in the midplane.

For the initial straight crack front, both CDFs present a relatively constant value in the central region of the mid-thickness, and display a significant decrease at the surface (Figure 8a, Figure 8b). In particular, the central values are approximately $\Delta\text{CTOD}_\text{p} \approx 7.2\text{e}-5$ mm and $\Delta\text{CTOD} \approx 2.6\text{e}-4$ mm, with respective decreases of 37% and 30% at the surface. The length of the surface region is around 0.2 mm for both CTOD-based CDFs. It should be noted that the same distribution has already been reported in ΔK_eff for the initial straight crack [16, 17].

When the crack starts to propagate (Figure 8a, Figure 8b), the arched shape of the CDF distribution is accentuated, because the CDFs increase in the central part and decrease close to the surface. This trend has also been reported under straight crack assumption [17], and it has attributed to a higher crack closure being developed close to the surface.

As the crack continues to propagate beyond the initial plastic envelope (Figure 8c, Figure 8d), $\Delta\text{CTOD}_\text{p}$ increases all along the mid-thickness and especially at the surface, whereas ΔCTOD increases almost exclusively at the surface. In that way, at a midplane crack advance of $1.8r_{\text{p,inimax}}$, both CDFs change from displaying maxima and minima at the two extremes, to presenting a valley close to the surface. That valley progressively moves away from the surface.

From $\Delta a_\text{mid}/r_{\text{p,inimax}} = 3.7$ onward (Figure 8e, Figure 8f), the through-the-thickness distribution of the CDFs is kept relatively constant, although the values in the thickness increase uniformly as the crack advances. Eventually, both CDFs converge to a non-iso distribution that is kept constant as the crack propagates. That stabilization occurs at $\Delta a_\text{mid} = 1.39$ mm ($7.32r_{\text{p,inimax}}$) for $\Delta\text{CTOD}_\text{p}$. The stable distribution presents a maximum value of $\Delta\text{CTOD}_\text{p} = 8.3\text{e}-5$ mm at the midplane, a minimum value (23% lower) at 0.1 mm from the surface, and an intermediate value (13% lower) at the surface. In the case of ΔCTOD, the stabilization occurs slightly later at $\Delta a_\text{mid} = 1.47$ mm ($7.75r_{\text{p,inimax}}$), and the stable CDF distribution displays: 1) a maximum value of $\Delta\text{CTOD} = 2.8\text{e}-4$ mm at the midplane, a minimum value (22% lower) at 0.08 mm from the surface and an intermediate value (5% lower) at the surface.

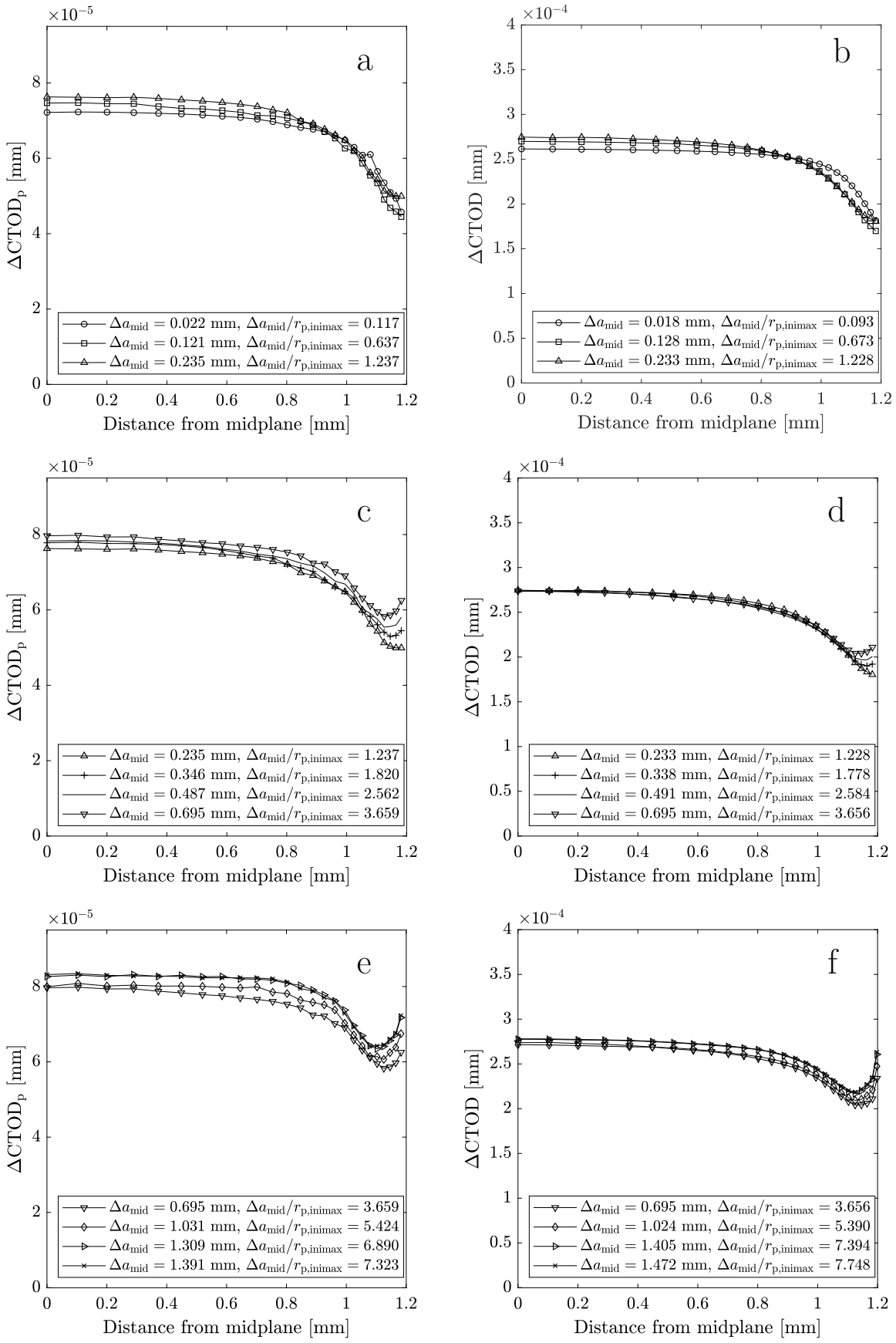

Figure 8: Evolution of $\Delta \mathrm{CTOD_p}$ (left) and $\Delta \mathrm{CTOD}$ (right) distributions with crack advance.

The identified non-iso CDF distribution is clearly represented by the evolution of the normalized CDFs at different locations in thickness (Figure 9). In fact, there are variations within the initial plastic zone for both $\Delta\text{CTOD}_\text{p}$ and ΔCTOD (especially in the surface region, 0.994 mm $\leq z \leq$ 1.2 mm). However, the normalized CDFs then gradually converge to saturated values different from 1.

As far as the authors know, this is the first time this trend has been identified, and its discovery contradicts the extensive literature [10, 13, 17, 18, 23]. Previous studied have examined different crack configurations regarding ΔK or ΔK_eff as CDF, so section 3 presents a theoretical analysis considering generic crack shapes and other fracture parameters.

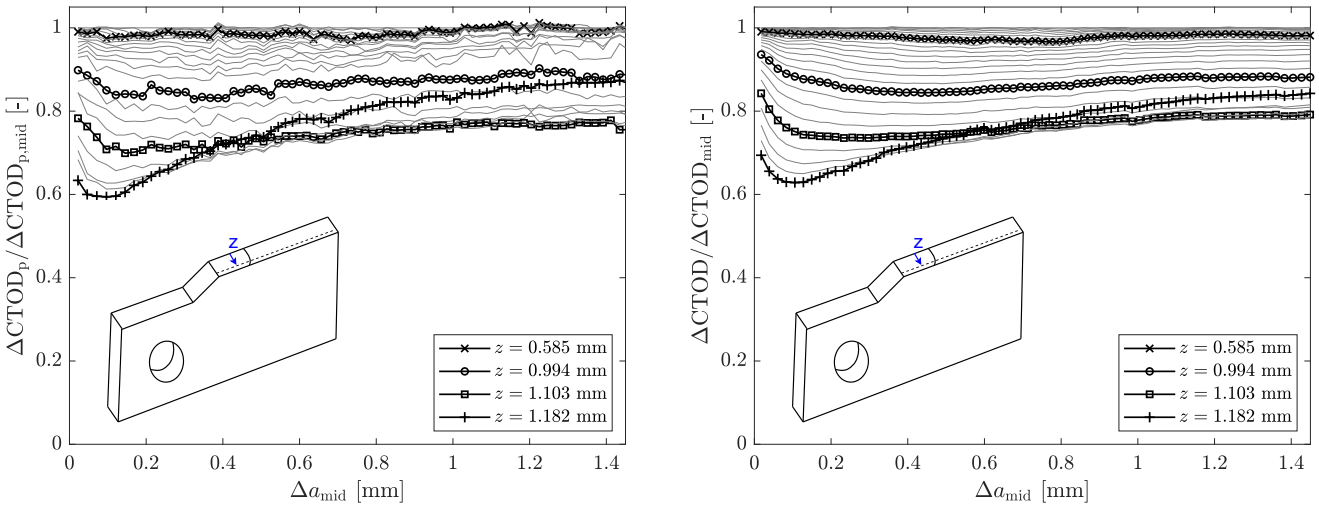

(a) $\Delta\text{CTOD}_\text{p}$ (b) ΔCTOD

Figure 9: Normalized CDF evolution against midplane advance for different thickness-locations.

3. Theoretical analysis of naturally growing generic cracks

Although unexpected considering the literature, it can be theoretically deduced that an iso-CDF distribution and a stable crack-shape growth are geometrically incompatible. Both the crack growth rate and CDF are defined perpendicular to the crack front and are univocally related by a crack growth law. Thus, the curvature of a non-straight crack front makes a crack growing with a stable shape (where every point advances the same in the global direction) incompatible with an iso-CDF distribution (where every point advances the same in the local perpendicular direction).

This section addresses various generic cracks that propagate under the action of different fracture parameters, to provide a practical demonstration of the above statement.

3.1. Strategy

Like the previous FE simulations, the present theoretical analysis is based on the multiple-degree-of-freedom approach (Figure 10), which consists of building the new crack front from 1) the new locations determined point by point and 2) a cubic splines interpolation. Crack growth was set to be

governed by a power-law relationship (Equation 1), which is representative for the most relevant linear elastic and elastic-plastic fracture parameters used as CDF.

$$\frac{\mathrm{d}a}{\mathrm{d}N} = C_1 \mathrm{CDF}^{C_2} \rightarrow \begin{cases} \frac{\mathrm{d}a}{\mathrm{d}N} = C\Delta K_{\mathrm{eff}}^{n} \\ \frac{\mathrm{d}a}{\mathrm{d}N} = C\Delta J^{n} \\ \frac{\mathrm{d}a}{\mathrm{d}N} = \beta\Delta\mathrm{CTOD} \\ \frac{\mathrm{d}a}{\mathrm{d}N} = \beta\Delta\mathrm{CTOD}_{\mathrm{p}} \end{cases} \tag{1}$$

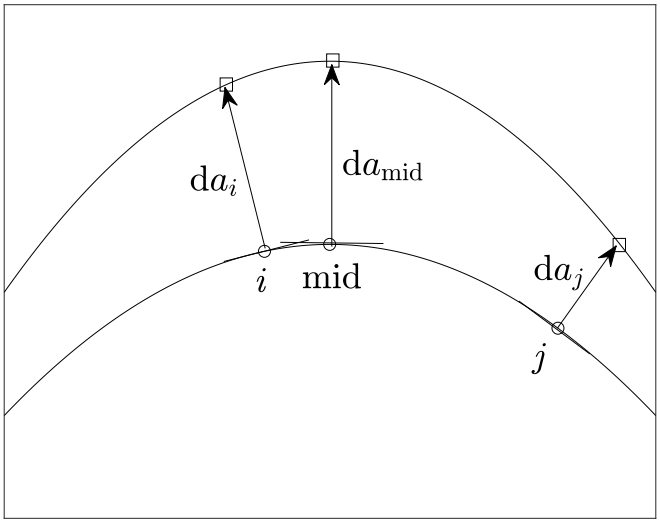

Figure 10: Illustration of multiple-degree-of-freedom approach.

In particular, Equation 2 (derived from Equation 1) determined the magnitudes of the local crack advances, by defining a small-enough midplane crack-advance ($\mathrm{d}a_{\mathrm{mid}}$) and using C_2 exponents ranging from 1 (suitable for $\Delta\mathrm{CTOD}_{(\mathrm{p})}$ [29]) to 4 (suitable for ΔK [31]). On the other side, Equation 3 determined the directions of those local crack advances, based on the local slopes (s_i), in turn, determined by the differentiation of the interpolating function.

$$\mathrm{d}a_i = \left(\frac{\mathrm{CDF}_i}{\mathrm{CDF}_{\mathrm{mid}}}\right)^{C_2} \mathrm{d}a_{\mathrm{mid}} \tag{2}$$

$$\vec{n}_i = \begin{bmatrix} \frac{-s_i}{\sqrt{1+s_i^2}} \\ \frac{1}{\sqrt{1+s_i^2}} \end{bmatrix}_{zx} \tag{3}$$

Finally, following the above formulation, Equation 4 (derived from Equation 2) back-calculated the CDF distribution required to provide the propagation between two given crack fronts.

$$\frac{\mathrm{CDF}_i}{\mathrm{CDF}_{\mathrm{mid}}} = \left(\frac{\mathrm{d}a_i}{\mathrm{d}a_{\mathrm{mid}}}\right)^{1/C_2} \tag{4}$$

3.2. Results

3.2.1. Crack growth under iso-CDF vs. crack growth under constant shape

Figure 11 shows two crack fronts obtained from a generic crack under two different conditions: 1) growth under iso-CDF distribution, where all the points advance the same distance in the local normal directions ($\mathrm{d}a_i = \mathrm{d}a_{\mathrm{mid}}$ from Equation 2), and 2) growth under constant crack shape, where all the points advance the same offset-distance in the global propagation direction. The dashed circles are drawn to highlight that the crack advances are identical in the two directions.

Both crack fronts only coincide in the midplane, where the local normal is parallel to the global propagation direction. For the rest of the points, the points' new locations are different for the two conditions. Therefore, this simple illustration demonstrates that, for curved crack fronts, crack growth under iso-CDF distribution and crack growth with constant crack shape are geometrically incompatible.

In fact, the only way to guarantee such compatibility is to have a crack front whose all local normal directions relate with the global propagation direction in the same angle, that is, to have a straight front.

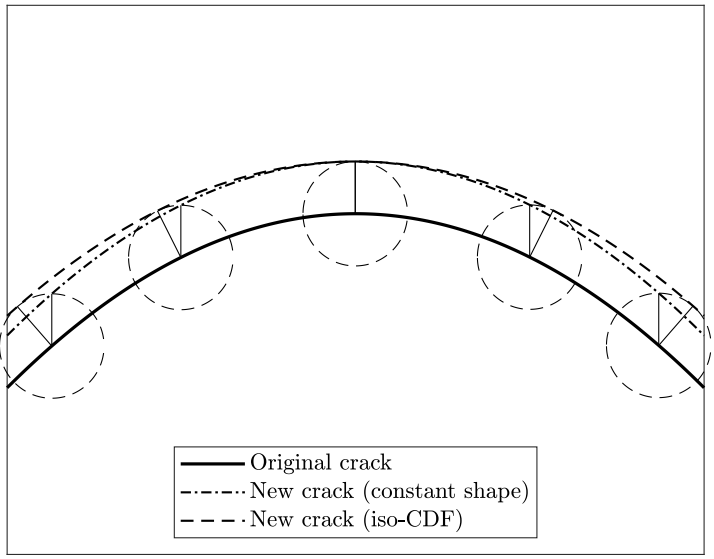

Figure 11: Crack growths 1) under iso-CDF and 2) under constant shape.

3.2.2. Crack shape evolution under iso-CDF distribution

Figure 12a shows the shape evolution determined for four different cracks under an assumed iso-CDF distribution (small-enough ≈ 1 µm advances). The first two cracks are initially ideal and follow respectively parabolic and elliptical shapes, the third crack is arbitrary, and the last one is the experimental beachmark measured at $\Delta a_{\mathrm{mid}} = 1.5$ mm. Note that the same evolution is predicted for any fracture parameter and material property (namely C_1 and C_2), because $\mathrm{d}a_i = \mathrm{d}a_{\mathrm{mid}}$ (from the particularization of Equation 2 to iso-CDF).

All the results display, from the beginning, a progressive flattening of the initial curved crack-fronts, with changes that gradually decrease. All the different crack-fronts reach similar "preferred paths"

after some extent of propagation, regardless of the initial tunneling distance and shape irregularities. In this sense, the flattening observed under iso-CDF contradicts wide experimental evidence [5, 6] that has found that fatigue cracks reach and consecutively preserve a stable shape.

In particular, Figure 12b shows the comparison between a beachmark directly measured at $\Delta a_{\text{mid}} = 11$ mm and the one predicted by the iso-CDF analysis starting from the experimental stable crack-front at $\Delta a_{\text{mid}} = 1.5$ mm. The difference is clear, because the analysis estimates a tunneling decrease from 264 µm at $\Delta a_{\text{mid}} = 1.5$ mm to 49 µm at $\Delta a_{\text{mid}} = 11$ mm, whereas in reality the tunneling is kept practically constant 264 µm *vs.* 269 µm.

Based on the above discovery, the FCG under an iso-CDF distribution is concluded to be physically inconsistent.

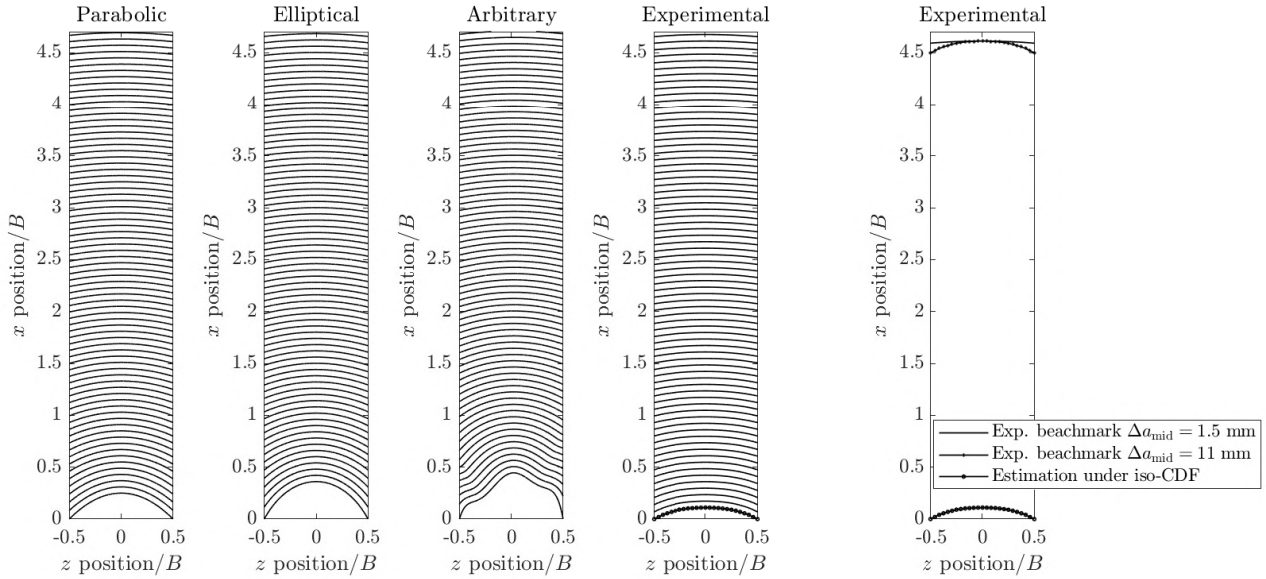

(a) FCG under iso-CDF

(b) Experimental *vs.* iso-CDF

Figure 12: Crack shape evolution under iso-CDF for different cracks.

3.2.3. CDF distribution for a stable crack shape

Figure 13a shows the CDF distributions calculated by Equation 4 to provide a crack growth with constant shape. The already presented crack-fronts are considered and various C_2 values ranging between the lower ($C_2 = 1$) and upper bounds ($C_2 = 4$) are assumed. All distributions are found to display a non-uniform (non-iso) profile that depends on both the crack shape and the power-law exponent. The higher the curvature or the lower the exponent, the more irregular the CDF distribution.

Figure 13b shows the CDF distributions determined by the simulations at the stable crack-shape regime and compares them to the profile back-calculated from the experimental beachmark ($C_2 = 1$ for linear laws). The three distributions display again a non-iso profile, characterized by a relatively constant central region and a valley close to the surface. As already observed at the beachmark comparison (Figure 6), the simulations indicate more abrupt changes at the surface than expected experimentally

and ΔCTOD yields better approximation through the thickness. The value $\mathrm{CDF_{min}/CDF_{mid}}$ is lower in the simulations (0.77 for ΔCTOD and 0.79 for $\Delta\mathrm{CTOD_p}$) than deduced from the experiment (0.89).

These results represent the definitive proof that, as long as the crack is curved (as expected at the stable growth regime [5, 6]) and FCG is driven by a power-law, a quasi-constant crack shape can only be maintained by a non-iso CDF distribution.

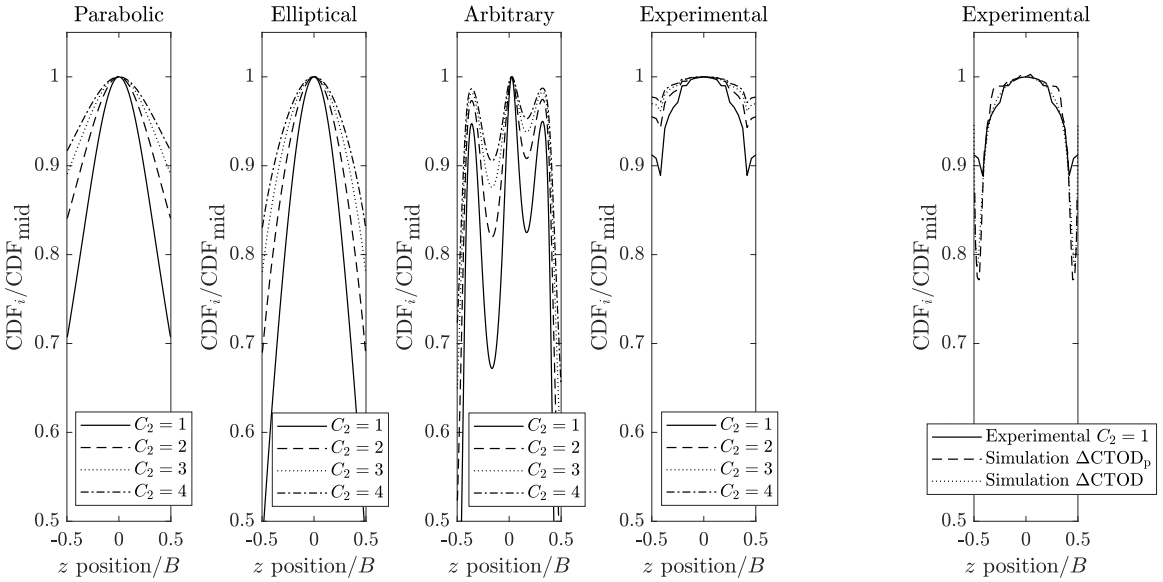

(a) Back-calculated CDF distributions

(b) Experimental *vs.* simulations

Figure 13: CDF distributions required to maintain constant crack shapes.

4. Conclusions

This work studied the evolution of naturally growing fatigue cracks, to establish the evolution of crack shapes and crack driving force distributions and their relationship.

To do this, the work simulated crack growth using an FCG propagation approach that 1) determines the CDF values by explicitly accounting for PICC (avoiding assumptions or analytical approximations for $P_{\mathrm{op}}/P_{\mathrm{max}}$), and 2) naturally builds the evolving crack shape from the local crack advances (avoiding postulated or mathematically fitted shapes). The approach had to be optimized to reduce the previous high computational cost, allowing to understand the whole FCG process up to the stable crack shape without artifacts.

Simulations were performed on the basis of CTOD-based fracture parameters considering the example of crack in a compact tension specimen. It was concluded that:

- There is an initial transitory stage where the through-the-thickness CDF distribution changes due to the development of the plastic wake. Consequently, the crack shape driven by the CDF distribution also changes.
- There is a final stage where the through-the-thickness CDF distribution converges to a non-iso (non-uniform) distribution. Such a non-iso CDF distribution produces a crack shape change that progressively decreases, therefore leading to a quasi-constant crack shape.
- The stable crack-shape predictions are validated by the good numerical-experimental correlation obtained at the tunneling of the stable crack (-4.17% error with $\Delta\mathrm{CTOD_p}$ and -8.93% with ΔCTOD).

In a second approach, motivated by the discovery of a quasi-constant crack shape provided by a non-iso CDF distribution, a theoretical analysis was performed. That analysis relied on crack growth predictions based on the multiple degree-of-freedom approach and power-law crack growth relationships, and considered generic CDFs and cracks. The analysis arrived at the following findings:

- Constant crack-shape growth and crack growth under iso-CDF distribution are incompatible for curved crack fronts, because the local normal directions of the crack do not coincide with the global propagation direction.
- The non-iso CDF distribution required by a constant crack-shape growth depends on the exponent that relates the fracture parameter and the crack growth rate and on the crack shape.
- An iso-CDF distribution is inconsistent at the stable fatigue crack growth regime, because such distribution produces a progressive flattening of the advancing crack front that contradicts the experimental evidence.

Acknowledgement

The authors would like to express their gratitude to the Spanish Ministry of Science and Innovation for the financial support given through project MCI-20-PID2019-105593GB-I00/AEI/10.13039/501100011033 and project CER-20190001 within the program "AYUDAS CERVERA PARA CENTROS TECNOLÓGICOS 2019". Ikerlan is currently certificated as CENTRO DE EXCELENCIA CERVERA.

References

[1] E. Wolf, Fatigue crack closure under cyclic tension, Engineering Fracture Mechanics 2 (1) (1970) 37 – 45. doi:https://doi.org/10.1016/0013-7944(70)90028-7.
URL http://www.sciencedirect.com/science/article/pii/0013794470900287

[2] J. Newman, A crack opening stress equation for fatigue crack growth, International Journal of Fracture 24 (4) (1984) R131–R135. doi:10.1007/BF00020751.

[3] J. C. Newman Jr, C. A. Bigelow, K. N. Shivakumar, Three-dimensional elastic-plastic finite-element analyses of constraint variations in cracked bodies, Tech. rep., National Aeronautics and Space Administration, Hampton (1993).

[4] T. Machniewicz, Fatigue crack growth prediction models for metallic materials. part ii: Strip yield model – choices and decisions, Fatigue & Fracture of Engineering Materials & Structures 36 (2012) 361 – 373. doi:10.1111/ffe.12009.

[5] M. Mahmoud, A. Hosseini, Assessment of stress intensity factor and aspect ratio variability of surface cracks in bending plates, Engineering Fracture Mechanics 24 (2) (1986) 207–221. doi:https://doi.org/10.1016/0013-7944(86)90052-4.
URL https://www.sciencedirect.com/science/article/pii/0013794486900524

[6] F. Bovecchi, L. Boni, D. Fanteria, L. Lazzeri, Assessment of a numerical strategy for fatigue growth and shape evolution of a corner crack from a pin-loaded hole, Engineering Fracture Mechanics 254 (2021) 107918. doi:https://doi.org/10.1016/j.engfracmech.2021.107918.
URL https://www.sciencedirect.com/science/article/pii/S001379442100343X

[7] R. McClung, H. Sehitoglu, On the finite element analysis of fatigue crack closure—2. numerical results, Engineering Fracture Mechanics 33 (2) (1989) 253 – 272. doi:https://doi.org/10.1016/0013-7944(89)90028-3.
URL http://www.sciencedirect.com/science/article/pii/0013794489900283

[8] X. Lin, R. Smith, Finite element modelling of fatigue crack growth of surface cracked plates: Part i: The numerical technique, Engineering Fracture Mechanics 63 (5) (1999) 503 – 522. doi:https://doi.org/10.1016/S0013-7944(99)00040-5.
URL http://www.sciencedirect.com/science/article/pii/S0013794499000405

[9] X. Lin, R. Smith, Finite element modelling of fatigue crack growth of surface cracked plates: Part ii: Crack shape change, Engineering Fracture Mechanics 63 (5) (1999) 523 – 540. doi:https:

//doi.org/10.1016/S0013-7944(99)00041-7.
URL http://www.sciencedirect.com/science/article/pii/S0013794499000417

[10] X. Lin, R. Smith, Finite element modelling of fatigue crack growth of surface cracked plates: Part iii: Stress intensity factor and fatigue crack growth life, Engineering Fracture Mechanics 63 (5) (1999) 541 – 556. doi:https://doi.org/10.1016/S0013-7944(99)00042-9.
URL http://www.sciencedirect.com/science/article/pii/S0013794499000429

[11] N. Couroneau, J. Royer, Simplified model for the fatigue growth analysis of surface cracks in round bars under mode i, International Journal of Fatigue 20 (10) (1998) 711–718. doi:https://doi.org/10.1016/S0142-1123(98)00037-1.
URL https://www.sciencedirect.com/science/article/pii/S0142112398000371

[12] R. Branco, F. Antunes, Finite element modelling and analysis of crack shape evolution in mode-i fatigue middle cracked tension specimens, Engineering Fracture Mechanics 75 (10) (2008) 3020 – 3037. doi:https://doi.org/10.1016/j.engfracmech.2007.12.012.
URL http://www.sciencedirect.com/science/article/pii/S0013794407004481

[13] M. Gilchrist, R. Smith, Finite element modelling of fatigue crack shapes, Fatigue & Fracture of Engineering Materials & Structures 14 (6) (1991) 617–626.

[14] Z. Wu, The shape of a surface crack in a plate based on a given stress intensity factor distribution, International Journal of Pressure Vessels and Piping 83 (3) (2006) 168–180. doi:https://doi.org/10.1016/j.ijpvp.2006.01.004.
URL https://www.sciencedirect.com/science/article/pii/S0308016106000196

[15] R. G. Chermahini, Three dimensional elastic-plastic finite element analysis of fatigue crack growth and closure, Ph.D. thesis, Old Dominion University (1986).

[16] C. Gardin, S. Fiordalisi, C. Sarrazin-Baudoux, J. Petit, 3d numerical study on how the local effective stress intensity factor range can explain the fatigue crack front shape, Advanced Materials Research Vols (2014) 295–300.

[17] C. Gardin, S. Fiordalisi, C. Sarrazin-Baudoux, J. Petit, Numerical simulation of fatigue plasticity-induced crack closure for through cracks with curved fronts, Engineering Fracture Mechanics 160 (2016) 213 – 225. doi:https://doi.org/10.1016/j.engfracmech.2015.11.023.
URL http://www.sciencedirect.com/science/article/pii/S0013794416301643

[18] R. BRANCO, D. M. RODRIGUES, F. V. ANTUNES, Influence of through-thickness crack shape on plasticity induced crack closure, Fatigue & Fracture of Engineering Materials & Structures 31 (2) (2008) 209–220. arXiv:https://onlinelibrary.wiley.com/doi/pdf/10.1111/j.1460-2695.2008.01216.x, doi:10.1111/j.1460-2695.2008.01216.x.
URL https://onlinelibrary.wiley.com/doi/abs/10.1111/j.1460-2695.2008.01216.x

[19] P. Yu, W. Guo, An equivalent thickness conception for prediction of surface fatigue crack growth life and shape evolution, Engineering Fracture Mechanics 93 (2012) 65 – 74. doi:https://doi.

org/10.1016/j.engfracmech.2012.06.008.
URL http://www.sciencedirect.com/science/article/pii/S0013794412002627

[20] P. Yu, W. Guo, An equivalent thickness conception for evaluation of corner and surface fatigue crack closure, Engineering Fracture Mechanics 99 (2013) 202 – 213. doi:https://doi.org/10.1016/j.engfracmech.2012.12.013.
URL http://www.sciencedirect.com/science/article/pii/S0013794412004742

[21] C.-Y. Hou, Simultaneous simulation of closure behavior and shape development of fatigue surface cracks, International Journal of Fatigue 30 (6) (2008) 1036 – 1046. doi:https://doi.org/10.1016/j.ijfatigue.2007.08.020.
URL http://www.sciencedirect.com/science/article/pii/S0142112307002514

[22] M.-H. Gozin, A.-K. Mehrdad, Quarter elliptical crack growth using three dimensional finite element method and crack closure technique, Journal of Mechanical Science and Technology 28 (2014) 2141–2151. doi:https://doi.org/10.1007/s12206-014-0503-x.
URL https://link.springer.com/article/10.1007/s12206-014-0503-x{#}citeas

[23] C. Gardin, S. Fiordalisi, C. Sarrazin-Baudoux, M. Gueguen, J. Petit, Numerical prediction of crack front shape during fatigue propagation considering plasticity-induced crack closure, International Journal of Fatigue 88 (2016) 68 – 77. doi:https://doi.org/10.1016/j.ijfatigue.2016.03.018.
URL http://www.sciencedirect.com/science/article/pii/S014211231630024X

[24] M. Escalero, M. Muniz-Calvente, H. Zabala, I. Urresti, R. Branco, F. Antunes, A methodology for simulating plasticity induced crack closure and crack shape evolution based on elastic–plastic fracture parameters, Engineering Fracture Mechanics 241 (2021) 107412. doi:https://doi.org/10.1016/j.engfracmech.2020.107412.
URL https://www.sciencedirect.com/science/article/pii/S0013794420309863

[25] V. Tvergaard, Effect of underloads or overloads in fatigue crack growth by crack-tip blunting, Engineering Fracture Mechanics 73 (7) (2006) 869 – 879.

[26] H. A. Tinoco, C. I. Cardona, T. Vojtek, P. Hutař, Finite element analysis of crack-tip opening displacement and plastic zones considering the cyclic material behaviour, Procedia Structural Integrity 23 (2019) 529 – 534.

[27] H. Xin, M. Veljkovic, Residual stress effects on fatigue crack growth rate of mild steel S355 exposed to air and seawater environments, Materials & Design 193 (2020) 108732.

[28] P. Cui, W. Guo, Crack-tip-opening-displacement-based description of three-dimensional elastic-plastic crack border fields, Engineering Fracture Mechanics 231 (2020) 107008.

[29] F. V. Antunes, R. Branco, P. A. Prates, L. Borrego, Fatigue crack growth modelling based on ctod for the 7050-t6 alloy, Fatigue & Fracture of Engineering Materials & Structures 40 (8) (2017) 1309–1320. arXiv:https://onlinelibrary.wiley.com/doi/pdf/10.1111/ffe.12582,

doi:10.1111/ffe.12582.
URL https://onlinelibrary.wiley.com/doi/abs/10.1111/ffe.12582

[30] F. Antunes, S. Serrano, R. Branco, P. Prates, Fatigue crack growth in the 2050-T8 aluminium alloy, International Journal of Fatigue 115 (2018) 79 – 88, crack tip fields 4. doi:https://doi.org/10.1016/j.ijfatigue.2018.03.020.
URL http://www.sciencedirect.com/science/article/pii/S0142112318301129

[31] P. Paris, F. Erdogan, A critical analysis of crack propagation laws (1963) 528–533.